JACS
JOURNAL OF THE AMERICAN CHEMICAL SOCIETY
pubs.acs.org/JACS

Article

Importance of Selective Quenching of the Triplet Excited State of Thermally Activated Delayed Fluorescence (TADF) Photosensitizers in Redox-Photosensitized Reactions: Case Studies on Photocatalytic CO_2 Reduction

Yusuke Tamaki,* Kei Kamogawa, Rei Inoue, Paola Ceroni, and Osamu Ishitani*

Cite This: https://doi.org/10.1021/jacs.5c10614

Read Online

ACCESS | Metrics & More | Article Recommendations | Supporting Information

ABSTRACT: Redox photosensitizers exhibiting thermally activated delayed fluorescence (TADF) are widely used in the various research fields. We investigated the roles of the singlet and triplet excited states of such molecules in photocatalytic CO_2 reduction. Two TADF compounds (**4DPAIPN** and **3DPAFIPN**) were used in combination with a manganese(I) complex as a catalyst and 1,3-dimethyl-2-phenyl-2,3-dihydro-1*H*-benzo[*d*]imidazole (BIH) and triethanolamine (TEOA) as sacrificial electron donors. In the case of **4DPAIPN**, the quantum yield of CO_2 reduction ($\Phi_{CO+HCOO-}$) was negatively correlated with the concentration of BIH, equaling 43.2% and 20.3% at [BIH] = 5 and 200 mM, respectively. The reduction of the singlet excited state by BIH afforded a singlet geminate ion pair, ^{1}(**4DPAIPN**$\bullet^-\cdots$BIH$\bullet^+$), which experienced a markedly faster backward electron transfer affording the ground state than the corresponding triplet, ^{3}(**4DPAIPN**$\bullet^-\cdots$BIH$\bullet^+$). The escape yield of the singlet state was approximately 10 times lower than that of the triplet state. High BIH concentrations favored the quenching of the singlet excited state and disfavored the formation of the triplet excited state, resulting in low photocatalytic efficiencies. Although the system with **3DPAFIPN** exhibited a similar tendency, the maximum $\Phi_{CO+HCOO-}$ was lower (11.9% at [BIH] = 10 mM) because of its greater oxidizing power resulting in the efficient quenching of its singlet excited state by TEOA. Based on these results, we extracted the reaction conditions and molecular designs of TADF photosensitizers suitable for constructing efficient photocatalysts, namely those minimizing the quenching of the singlet excited state and maximizing the quenching of the triplet excited state.

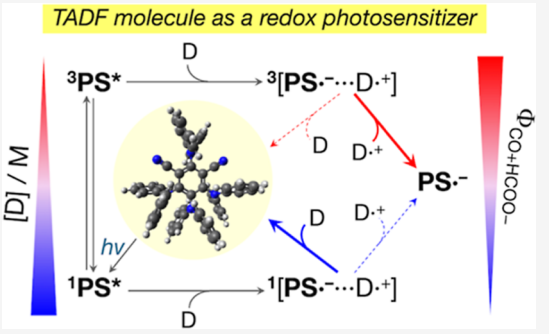

1. INTRODUCTION

Redox-photosensitized (RPS) reactions, also known as photoredox catalytic reactions, have attracted considerable attention, especially in the fields of artificial photosynthesis[1,2] and organic synthesis.[3,4] Redox photosensitizers (**PS**s, photoredox catalysts) initiate RPS reactions. For example, the **PS** absorbs a photon, and the resulting excited state (**PS***) is reductively quenched by an electron donor to afford a one-electron-reduced species (OERS, **PS**$\bullet^-$), which donates an electron to the substrate or catalyst. Therefore, the efficiency (quantum yield) of **PS**$\bullet^-$ formation substantially affects the overall efficiency of the RPS reactions.

Most **PS**s can be classified as complexes of heavy transition metals, e.g., Ru(II),[3,5−12] Os(II),[13−15] Ir(III),[16−18] and Re(I)[19,20] (Class 1), and organic compounds[21−29] and complexes of lighter metals, e.g., Cu[30−34] and Zn[35−39] (Class 2). The metal complexes in the Class 1 fulfill the requirements as **PS** relatively in good balance and are frequently used in numerous RPS reactions. In particular, their long excited-state lifetimes are contributed by the heavy-atom effect of metal centers inducing rapid intersystem crossing and producing long-lived triplet excited states, quantitatively. Previously, the factor mainly determining the quantum yield of **PS**$\bullet^-$ formation in the photochemical reduction of Class 1 **PS**s was identified as the high oxidation power of **PS*** using 1,3-dimethyl-2-phenyl-2,3-dihydro-1*H*-benzo[*d*]imidazole (BIH, a sacrificial electron donor frequently employed in RPS reactions).[40,41] This high oxidation power results in a large distance between **PS**$\bullet^-$ and BIH$\bullet^+$ in the geminate ion pair ^{3}(**PS**$\bullet^-\cdots$BIH$^{\bullet+}$) formed immediately after the photoinduced electron transfer and slow back electron transfer between these ion radicals in the geminate ion pair. Other factors, such as the heavy-atom effect (which can induce rapid back electron transfer in the triplet geminate ion pair) and the oxidation potential of **PS**$\bullet^-$, were

Received: June 23, 2025
Revised: August 19, 2025
Accepted: August 20, 2025

found to have minor effects on the quantum yield of photochemical **PS**•$^-$ formation.

Although Zn porphyrins are frequently used as **PS**s for RPS reactions, the quantum yields of **PS**•$^-$ formation are generally low because of the short lifetimes of the excited Zn porphyrins (several nanoseconds, the singlet excited state without a heavy metal experiences a slow intersystem crossing) and the resulting low quenching efficiency of excited Zn porphyrin by electron donors or acceptors.[35−37] Kuramochi et al. reported that attachment of a Re complex proximal to the Zn porphyrin induces the heavy-atom effect of the Re(I) ion to the Zn porphyrin unit to increase its photosensitizer ability in photocatalytic CO_2 reduction reactions.[38,39]

Large-scale applications require **PS**s comprising earth-abundant elements only. In addition, metal-free photoredox catalysts may be useful for pharmaceutical syntheses, helping avoid contamination with toxic metals. Therefore, purely organic **PS**s have been extensively developed, with early examples involving species driving the photocatalytic reduction of CO_2, such as cyanoanthracene[23] and oligo(*p*-phenylenes).[24,25] However, these compounds suffer from short excited-state lifetimes and poor visible-light absorption. Recently, purpurin[26,27] and phenazine[28,29] derivatives have been used as organic photosensitizers because of their strong visible-light absorption and ability to populate long-lived triplet excited states, respectively.

Molecules exhibiting thermally activated delayed fluorescence (TADF), originally developed as light-emitting materials for electroluminescent devices,[42−44] are frequently used as **PS**s in organic synthesis[21,22,45,46] and photocatalytic CO_2 reduction.[47−51] Heteroleptic Cu(I) complexes with diimine and phosphine ligands also show TADF properties and have been actively investigated as **PS**s for photocatalytic CO_2 reduction despite containing a transition metal (Cu).[30−34]

In numerous organic TADF molecules, electron-donating and -accepting moieties are highly twisted to minimize the energy gap between the lowest singlet and triplet excited states.[52] Therefore, both intersystem crossing (ISC) and reverse intersystem crossing (RISC) are accelerated, and a high population of the long-lived triplet excited state is achieved at ambient temperature. Long-lived excited states are one of the most important features of **PS**s. For example, 1,2,3,5-tetrakis(carbazol-9-yl)-4,6-dicyanobenzene was first used as a TADF **PS** for CO_2 reduction.[47,48] However, the quantum yield for CO_2 reduction was low (<5%), and the photoinduced electron transfer processes in this system are not explored in detail. Previously, we examined the performances of five organic compounds exhibiting TADF as **PS**s for photocatalytic CO_2 reduction in the presence of a Mn(I) complex catalyst (**Mn** in Chart 1) and BIH as a sacrificial electron donor, revealing that **4DPAIPN** and **3DPAFIPN** (Chart 1) as **PS**s displayed high performances because of their strong visible-light absorption and appropriate redox potentials.[53] In the case of **4DPAIPN**, CO_2 was photocatalytically reduced to CO and $HCOO^-$ with a quantum yield ($\Phi_{CO+HCOO-}$) of 22.8% and turnover number ($TON_{CO+HCOO-}$) of 665 in the presence of 0.1 M BIH upon irradiation at λ_{max} = 470 nm in *N*,*N*-dimethylacetamide (DMA)−triethanolamine (TEOA) solution. The corresponding reaction mechanism is summarized in Scheme 1.

Chart 1. Structures of the molecules exhibiting thermally activated delayed fluorescence (4DPAIPN and 3DPAFIPN) and catalyst (Mn) used in this study.

Scheme 1. Mechanism of Photocatalytic CO_2 Reduction in the Presence of 4DPAIPN (Redox Photosensitizer, PS), 1,3-Dimethyl-2-phenyl-2,3-dihydro-1*H*-benzo[*d*]imidazole (BIH, Electron Donor), and Mn (Catalyst); Lifetimes of the Excited States of 4DPAIPN (τ) and Quenching Rate Constants (k_q)

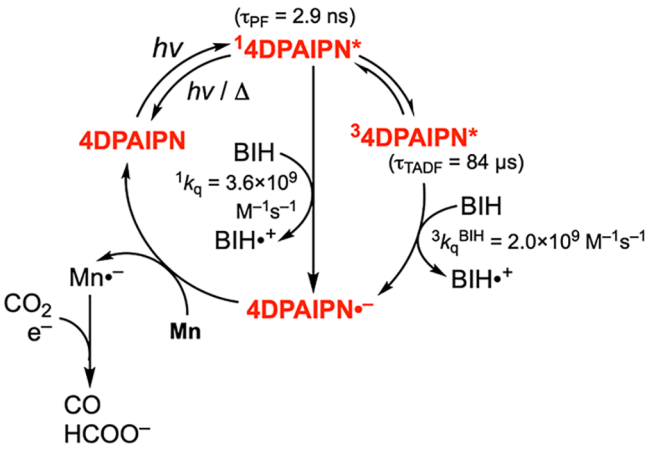

Although these results demonstrate the usefulness of TADF molecules as **PS**s, the roles, properties, and contributions of the singlet (^{1}**PS***) and triplet (^{3}**PS***) excited states of **PS**s in RPS reactions have not been clarified. The lowest singlet and triplet excited states of TADF molecules have very different properties due to the difference in their spin states: the former has a shorter lifetime but stronger reducing and oxidizing power because of its higher excitation energy ($^1E_{00}$ in Table 1),

Table 1. Reduction Potentials of 4DPAIPN and 3DPAFIPN in Ground and Excited States

	$E_{1/2}^{red}$/V[a]	$^1E_{00}$/eV[b]	$^3E_{00}$/eV[c]	$E(^1$**PS***/**PS**•$^-$)/V[d]	$E(^3$**PS***/**PS**•$^-$)/V[e]
4DPAIPN	−2.08	2.59[f]	2.42[f]	+0.51	+0.34
3DPAFIPN	−1.94	2.68[g]	2.47[g]	+0.74	+0.53

[a]Reduction potentials in ground states vs Fc^+/Fc. [b]0−0 excitation energies of the lowest singlet excited states. [c]0−0 excitation energies of the lowest triplet excited states. [d]Reduction potentials in singlet excited states calculated as $E(^1$**PS***/**PS**•$^-$) = $E_{1/2}^{red}$ + $^1E_{00}$ vs Fc^+/Fc. [e]Reduction potentials in triplet excited states calculated as $E(^3$**PS***/**PS**•$^-$) = $E_{1/2}^{red}$ + $^3E_{00}$ vs Fc^+/Fc. [f]Ref 45. [g]Ref 22.

whereas the latter has a longer lifetime but weaker reducing and oxidizing power because of its lower excitation energy ($^3E_{00}$). The geminate ion pairs formed upon electron transfer from the electron donor to the singlet and triplet excited states of the **PS** are singlet and triplet states, respectively, which might affect photocatalysis.[21,54−57] However, to the best of our knowledge, the effects of the spin states of the excited states

https://doi.org/10.1021/jacs.5c10614
J. Am. Chem. Soc. XXXX, XXX, XXX−XXX

and geminate ion pairs on photocatalytic reactions promoted by TADF **PS**s have not been examined.

Therefore, we herein investigated the characteristics of the above-mentioned TADF **PS**s (**4DPAIPN** and **3DPAFIPN**), including the roles of their singlet and triplet excited states, in photocatalytic CO_2 reduction. Based on the obtained information, we used **4DPAIPN** as the **PS**, **Mn** as the catalyst, and BIH as the reductant to achieve a high $\Phi_{CO+HCOO-}$ of 43.2%, which is the highest quantum yield among those reported for photocatalytic systems with organic TADF molecules as **PS**s.

2. RESULTS AND DISCUSSION

2.1. Case Study of 4DPAIPN. **4DPAIPN** displayed both prompt fluorescence (PF) and TADF at λ_{em}^{max} = 527 nm with emission lifetimes of τ_{PF} = 2.9 ns and τ_{TADF} = 84 μs in a degassed DMA solution, respectively.[53] The UV−vis absorption and emission spectra of **4DPAIPN** are shown as red solid and dotted lines in Figure 1, respectively. In contrast, no

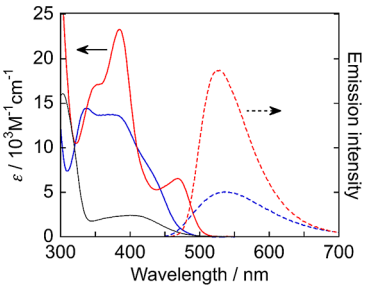

Figure 1. UV−vis absorption and emission spectra of **4DPAIPN** (red) and **3DPAFIPN** (blue) along with the absorption spectrum of **Mn** (black) measured in DMA.

phosphorescence originating from the triplet excited state (^{3}**4DPAIPN***) was observed at room temperature. The emission in air was notably weaker (Φ_{em}^{air} = 6.8%) than that in Ar (Φ_{em}^{Ar} = 48.9%), and τ_{TADF} was notably shorter in air (Figure 2), i.e., τ_{TADF}^{air} = 0.63 μs, $\tau_{TADF}^{air}/\tau_{TADF}$ = 7.5 × 10^{-3}. TADF was largely quenched by atmospheric O_2 (which has a triplet ground state) because it occurred via ^{3}**4DPAIPN*** (Figure 2b,c). The decay lifetime of the prompt fluorescence did not change in air, which indicated that the singlet excited state (^{1}**4DPAIPN***) was not quenched by atmospheric O_2 (Figure 2a). Since almost all of TADF (99.3%) was quenched by O_2 in air, we can estimate the quantum yield of TADF as $\Phi_{em}^{Ar} - \Phi_{em}^{air}$ = 48.9−6.8 = 42.1(%). Since, in addition, both PF and TADF occur from ^{1}**4DPAIPN*** and the ratios between the nonradiative and radiative processes should be same, the ratio between the excited-state deactivation processes (DAPs) involving ^{1}**4DPAIPN*** produced just after the photoexcitation of **4DPAIPN** and via RISC from ^{3}**4DPAIPN*** was estimated as DAP(PF)/DAP(TADF) ≈ 6.8/(48.9−6.8) = 14/86 in the absence of a quencher.

This phenomenon is typical of TADF-type **PS**s, that is, the singlet and triplet excited states have very different lifetimes and possibly contribute to RPS reactions. In contrast, in the case of the frequently used Class 1 **PS**s, only the triplet excited state induces photochemical electron transfer because of the fast intersystem crossing completed within several tens of femtoseconds, a time period too short for the singlet excited state to diffusionally contact a substrate, such as BIH (typically 100 mM). In the photocatalytic system with **4DPAIPN** as a photosensitizer (Scheme 1), both ^{1}**4DPAIPN*** and ^{3}**4DPAIPN*** were reductively quenched by BIH, with the corresponding rate constants equaling ^1k_q = 3.6 × 10^9 M^{-1}s^{-1} and $^3k_q^{BIH}$ = 2.0 × 10^9 M^{-1}s^{-1}, respectively (Figure S2). As the reductive quenching of ^{1}**4DPAIPN*** competes against not only radiative and nonradiative decays to the ground state but also against ISC to ^{3}**4DPAIPN***, the reductive quenching of ^{1}**4DPAIPN*** lowers the amount of the produced ^{3}**4DPAIPN***. This phenomenon should have a strong influence on the OERS formation processes of **4DPAIPN** and photocatalysis. In other words, photocatalytic reactions mediated by TADF molecules (such as **4DPAIPN**) as **PS**s are often initiated by two reductive quenching processes (those involving ^{1}**PS*** and ^{3}**PS***), which interactively proceed in parallel during photocatalytic reactions. To the best of our knowledge, no detailed analysis of the reductive quenching processes of TADF molecules and their effects on photocatalytic reactions has been performed; therefore, we investigated photocatalytic CO_2 reduction using **4DPAIPN** as a **PS** from this viewpoint. For this purpose, we systematically changed the quenching ratio between ^{1}**4DPAIPN*** and ^{3}**4DPAIPN*** by controlling the concentration of the reductant (BIH), as the lifetimes of ^{1}**4DPAIPN*** and ^{3}**4DPAIPN*** are very different (Scheme 1).

Figure 3 displays the photocatalytic production of CO and $HCOO^-$ upon the irradiation of DMA solutions containing **4DPAIPN** (50 μM), **Mn** (50 μM), TEOA (1.5 M), and BIH (10 mM or 100 mM) at λ_{ex} = 480 nm. In the case of 10 mM BIH, notably larger amounts of $HCOO^-$ (Φ_{HCOO-} = 30.0 ± 2.0%) and CO (Φ_{CO} = 12.2 ± 0.2%) were produced despite the lower concentration of BIH, and the total quantum yield for CO_2 reduction ($\Phi_{CO+HCOO-}$ = 42.2 ± 2.2%) was 1.85 times

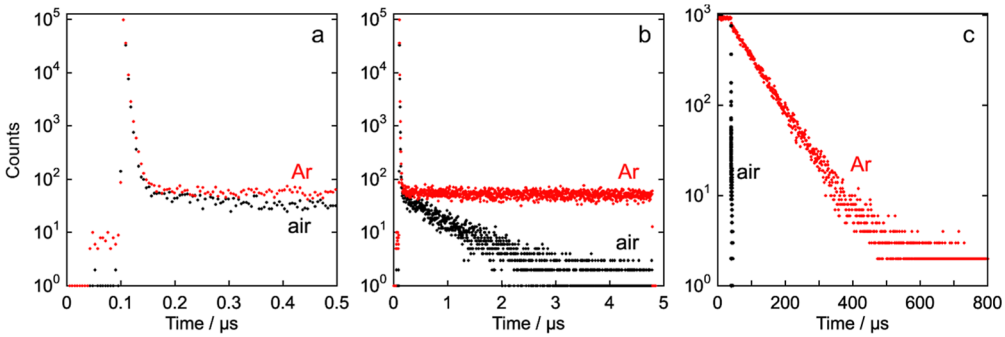

Figure 2. Emission intensity decays (λ_{em} = 530 nm) of 10 μM **4DPAIPN** in Ar-saturated and air-equilibrated DMA within the time ranges of (a) 0−0.5 μs, (b) 0−5 μs, and (c) 0−800 μs. The excitation wavelength equaled 444 nm ((a,b) and black plots in (c)) or 459 nm (red plots in (c)).

https://doi.org/10.1021/jacs.5c10614
J. Am. Chem. Soc. XXXX, XXX, XXX−XXX

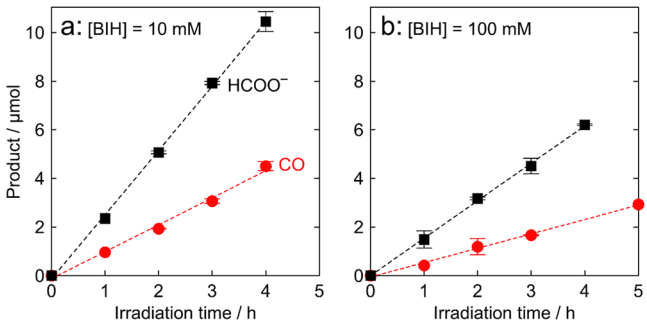

Figure 3. Photocatalytic production of CO (●) and $HCOO^-$ (■) using (a) 10 mM or (b) 100 mM of BIH: CO_2-saturated DMA solutions (4 mL) containing **4DPAIPN** (50 μM), **Mn** (50 μM), BIH and TEOA (1.5 M) were irradiated at λ_{ex} = 480 nm. Light intensity = 5.0×10^{-9} Einstein·s^{-1}.

that observed for 100 mM BIH ($\Phi_{CO+HCOO-}$ = 22.8 ± 1.5%). The $\Phi_{CO+HCOO-}$ values at various concentrations of BIH are summarized in Table 2 (Figure S3). The highest $\Phi_{CO+HCOO-}$ value (43.2%) was obtained at [BIH] = 5 mM, which is the highest quantum yield in the reported for photocatalytic CO_2 reduction reactions mediated by purely organic **PS**s. In the cases using high concentration of the added BIH (≥100 mM, i.e., ≥400 μmol contained in the reaction solutions), the concentrations of BIH can be assumed to be constant during the measurements of the quantum yield (Table 2). On the other hand, in the cases using 5 mM of BIH (20 μmol), after 2 h irradiation for example, about 5 μmol of BIH was consumed (Figure 3). However, the formation speeds of formate and CO did not clearly decrease. Therefore, even in the lower concentrations of BIH than 5 mM of BIH, high quantum yields of CO_2 reduction should be kept.

The fact that higher $\Phi_{CO+HCOO-}$ values were obtained at lower BIH concentrations appears "peculiar", as lower BIH concentrations resulted in lower quenching ratios of emission (η_q in eq 1) from excited **4PDAIPN** (η_q = 97% at [BIH] = 200 mM vs 88% at [BIH] = 5 mM) (Table 2 and Figure S4).

$$\eta_q = (I_0 - I)/I_0 \quad (1)$$

where I and I_0 are the emission intensities in the presence and absence of reductants (BIH and TEOA), respectively.

To rationalize the "unusual" dependence of $\Phi_{CO+HCOO-}$ on the concentration of BIH, the reductive quenching processes were investigated in detail, especially based on the spin states of the excited **4DPAIPN**. Scheme 2 illustrates the reductive quenching processes of ^{1}**4DPAIPN*** and ^{3}**4DPAIPN*** affording the corresponding geminate ion pairs, i.e. ^{1}(**4DPAIPN**$\bullet^-\cdots$BIH$^{\bullet+}$), ^{3}(**4DPAIPN**$\bullet^-\cdots$BIH$^{\bullet+}$), and ^{3}(**4DPAIPN**$\bullet^-\cdots$TEOA$^{\bullet+}$). As previously reported, ^{3}**4DPAIPN*** was reductively quenched by both BIH and TEOA, whereas ^{1}**4DPAIPN*** was quenched only by BIH because of its notably shorter lifetime (τ_{PF} = 2.9 ns) and lower reducing power of TEOA (E = +0.57∼+0.82 V vs SCE[58] ≈ + 0.19∼+0.44 V vs Fc^+/Fc) compared with that of BIH ($E_{1/2}$(BIH$\bullet^+$/BIH) = − 0.11 V vs Fc^+/Fc[40]).[53]

Based on Scheme 2, the time courses of the excited-state concentrations are described by eqs 2 and 3.

$$d[^1\textbf{4DPAIPN}^*]/dt = -(k_r + k_{nr} + k_{ISC} + {}^1k_q[\text{BIH}])[^1\textbf{4DPAIPN}^*] + k_{RISC}[^3\textbf{4DPAIPN}^*] \quad (2)$$

$$d[^3\textbf{4DPAIPN}^*]/dt = k_{ISC}[^1\textbf{4DPAIPN}^*] - (k_{RISC} + {}^3k_q^{BIH}[\text{BIH}] + {}^3k_q^{TEOA}[\text{TEOA}])[^3\textbf{4DPAIPN}^*] \quad (3)$$

where k_r and k_{nr} are the rate constants of the radiative and nonradiative deactivation from ^{1}**4DPAIPN***, respectively, and k_{ISC} and k_{RISC} are the rate constants of intersystem crossing from ^{1}**4DPAIPN*** and reversed intersystem crossing from ^{3}**4DPAIPN***, respectively. The rate constants of the reductive quenching of ^{1}**4DPAIPN*** by BIH and ^{3}**4DPAIPN*** by BIH and TEOA are denoted as ^1k_q, $^3k_q^{BIH}$, $^3k_q^{TEOA}$, respectively. The radiative decay from ^{3}**4DPAIPN*** was excluded because phosphorescence was not observed, as described above, and nonradiative decay was negligible because it was markedly slower than the quenching processes of BIH and TEOA for the high concentrations of BIH and TEOA used in our experiments. We can assume that the concentrations of BIH and TEOA were constant during the kinetic experiments, i.e., lifetime and quenching measurements of fluorescence. In the absence of quenchers, i.e., at [BIH] = [TEOA] = 0, k_r, k_{nr}, k_{ISC}, and k_{RISC} were calculated from $\Phi_{PF} \approx \Phi_{em}^{air}$ = 6.8%, $\Phi_{TADF} \approx \Phi_{em}^{Ar} - \Phi_{em}^{air}$ = 42.1%, τ_{PF} = 2.9 ns, and τ_{TADF} = 84 μs as follows (eqs 4−7, see Supporting Information for detailed kinetic calculations)

$$k_r = \Phi_{PF}/\tau_{PF} = 2.2 \times 10^7\ s^{-1} \quad (4)$$

$$k_{nr} = k_r\{1 - (\Phi_{PF} + \Phi_{TADF})\}/(\Phi_{PF} + \Phi_{TADF}) = 2.3 \times 10^7\ s^{-1} \quad (5)$$

Table 2. Quantum Yields (%) of CO_2 Reduction and Calculated Quantum Yields of Reductive Quenching Processes at Various BIH Concentrations in Systems With 4DPAIPN

[BIH]/mM	$\Phi_{CO+HCOO-}$ [a]	Φ_{CO} [a]	Φ_{HCOO-} [a]	η_q [b]	$^1\Phi_q^{BIH}$	$^3\Phi_q^{BIH}$	$^3\Phi_q^{TEOA}$	Φ_q^{total} [c]
5	43.2	12.2	31.0	88	5.1	82	0.4	87
10	42.2 ± 2.2	12.2 ± 0.2	30.0 ± 2.0	88	9.7	78	0.2	88
50	32.7	8.5	24.2	90	35	56	0.03	91
100	22.8 ± 1.5	5.9 ± 0.2	16.9 ± 1.3	92	52	42	0.01	94
200	20.3	4.8	15.5	97	68	28	0.003	96

[a]Quantum yields for CO_2 reduction: CO_2-saturated DMA solutions (4 mL) containing **4DPAIPN** (50 μM), **Mn** (50 μM), BIH, and TEOA (1.5 M) were irradiated at λ_{ex} = 480 nm and light intensity = 5.0×10^{-9} Einstein·s^{-1}. [b]Emission quenching fraction determined from the emission spectra measured in CO_2-saturated DMA solutions containing BIH and TEOA (1.5 M) as $\eta_q = (I_0 - I)/I_0$, where I_0 is the emission intensity in the absence of BIH and TEOA and I is the emission intensity in the presence of BIH (various concentrations) and TEOA (1.5 M). [c]$\Phi_q^{total} = {}^1\Phi_q^{BIH} + {}^3\Phi_q^{BIH} + {}^3\Phi_q^{TEOA}$.

https://doi.org/10.1021/jacs.5c10614
J. Am. Chem. Soc. XXXX, XXX, XXX−XXX

Scheme 2. Reductive Quenching Processes of the Excited States of 4DPAIPN by BIH or TEOA to Form Geminate Ion Pairs Along With the Competitive Deactivation Processes of Excited States

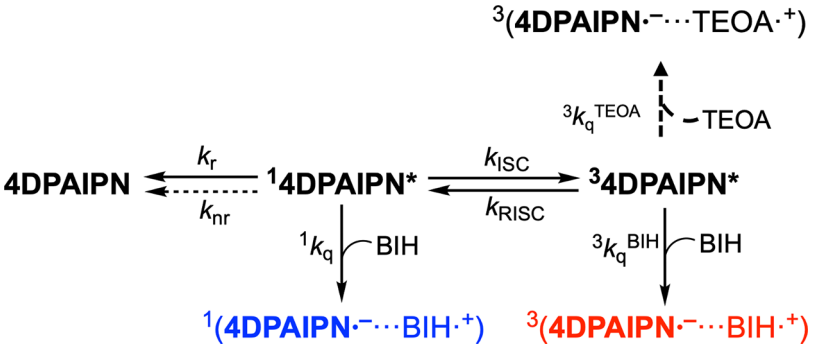

$$k_{ISC} = 1/\tau_{PF} - (k_r + k_{nr}) = 2.9 \times 10^8\ s^{-1} \quad (6)$$

$$k_{RISC} = 1/\{\tau_{PF}\tau_{TADF}(k_r + k_{nr})\} = 1.0 \times 10^5\ s^{-1} \quad (7)$$

The thus obtained values are consistent with those previously determined using the photophysical measurements of **4DPAIPN** in acetonitrile,[59] which supports the validity of this analysis. The reductive quenching rate of ^{1}**4DPAIPN***, ^1k_q[BIH] = $3.6 \times 10^9 \times 5 \times 10^{-3} = 1.8 \times 10^7\ s^{-1}$, at a lower BIH concentration (5 mM) was comparable with those of radiative and nonradiative decays (eqs 4 and 5), with the intersystem crossing rate (eq 6) exceeding the combined rate of these processes ($(2.2 + 2.3 + 1.8) \times 10^7 = 6.3 \times 10^7\ s^{-1}$) 4.6-fold. In the case of 100 mM BIH, the reductive quenching of ^{1}**4DPAIPN*** was notably faster (^1k_q[BIH] = $3.6 \times 10^8\ s^{-1}$), and the intersystem crossing (eq 6) was slower than the combined rates of the other processes ($(2.2 + 2.3 + 36) \times 10^7 = 4.1 \times 10^8\ s^{-1}$). Given that the reversed intersystem crossing process from ^{3}**4DPAIPN*** (eq 7) was notably slower than the reductive quenching of ^{3}**4DPAIPN*** even in the case of 5 mM BIH (^3k_q[BIH] = $2.0 \times 10^9 \times 5 \times 10^{-3} = 1.0 \times 10^7\ s^{-1}$), ^{1}**4DPAIPN** reproduced from ^{3}**4DPAIPN*** was assumed not to contribute to the following processes and omitted from the discussion (as in the case of **3DPAFIPN** discussed later). Based on these rate constants along with those of the reductive quenching processes (^1k_q, $^3k_q^{BIH}$, and $^3k_q^{TEOA}$) determined by quenching experiments (Figure S2) and previously reported emission lifetimes, the quantum yields for the reductive quenching of ^{1}**4DPAIPN*** and ^{3}**4DPAIPN*** by BIH to form ^{1}(**4DPAIPN**•$^-$···BIH$^{•+}$) and ^{3}(**4DPAIPN**•$^-$···BIH$^{•+}$), i.e., $^1\Phi_q^{BIH}$ and $^3\Phi_q^{BIH}$, respectively, were calculated as functions of the BIH concentration (eqs S12 and S13 in Supporting Information). Figure 4 shows the results with the quantum yields of photocatalytic CO_2 reduction ($\Phi_{CO+HCOO-}$) for various BIH concentrations. The quantum yield for the reductive quenching of ^{3}**4DPAIPN*** by TEOA to form ^{3}(**4DPAIPN**•$^-$···TEOA$^{•+}$) was very small ($^3\Phi_q^{TEOA}$ < 1% at [BIH] = 5−200 mM), indicating that the contribution of TEOA to the production of **4DPAIPN**•$^-$ and photocatalytic CO_2 reduction could be ignored under these conditions. The sum of the quantum yields for reductive quenching by BIH and TEOA ($\Phi_q^{total} = {}^1\Phi_q^{BIH} + {}^3\Phi_q^{BIH} + {}^3\Phi_q^{TEOA}$) well agreed with the emission quenching fraction of BIH and TEOA (η_q) determined experimentally (Figure S4), which supported the appropriateness of this quantum yield calculation (Table 2). Notably, with the increasing [BIH], $^1\Phi_q^{BIH}$ increased, whereas $^3\Phi_q^{BIH}$ decreased because of the concomitant decrease in the total amount of ^{3}**4DPAIPN*** via the reductive quenching of ^{1}**4DPAIPN*** (Figure 4).

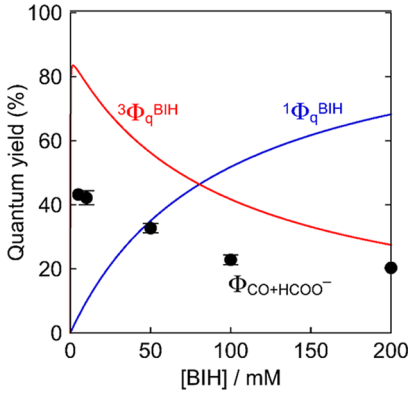

Figure 4. Quantum yields for CO_2 reduction ($\Phi_{CO+HCOO-}$, ●) and calculated quantum yields for reductive quenching from singlet ($^1\Phi_q^{BIH}$, blue line) and triplet excited states ($^3\Phi_q^{BIH}$, red line) to form ^{1}(**4DPAIPN**•$^-$···BIH$^{•+}$) and ^{3}(**4DPAIPN**•$^-$···BIH$^{•+}$), respectively, as functions of the BIH concentration.

As shown in Figure 4, the dependence of $\Phi_{CO+HCOO-}$ on the concentration of BIH was similar to that observed for $^3\Phi_q^{BIH}$ and opposite to that observed for $^1\Phi_q^{BIH}$. This behavior indicates that the contribution of the reductive quenching of ^{1}**4DPAIPN*** to photocatalysis should be substantially lower than that of ^{3}**4DPAIPN***. The reductive quenching of ^{1}**4DPAIPN*** should decrease the total produced amount of ^{3}**4DPAIPN*** and lower the efficiency of photocatalysis. The main reason for these drastic effects can be understood based on the difference in the spin states between the geminate ion pairs produced by electron transfer from BIH to ^{1}**4DPAIPN*** and ^{3}**4DPAIPN***, which should inherit the spin states of the excited states of **4DPAIPN**. Therefore, the reductive quenching of ^{1}**4DPAIPN*** and ^{3}**4DPAIPN*** by BIH produces ^{1}(**4DPAIPN**•$^-$···BIH$^{•+}$) and ^{3}(**4DPAIPN**•$^-$···BIH$^{•+}$), respectively (Scheme 3). These geminate ion pairs were mainly deactivated via backward electron transfer to regenerate **4DPAIPN** and BIH. The spin state should strongly affect the rate of this process, that is, the spin-forbidden backward electron transfer in ^{3}(**4DPAIPN**•$^-$···BIH$^{•+}$) should be much slower than the spin-allowed one in ^{1}(**4DPAIPN**•$^-$···BIH$^{•+}$) (Scheme 3). Since, a larger amount of ^{1}**4DPAIPN*** was reductively quenched at higher BIH concentrations, the more rapid backward electron transfer lowering the quantum yield of photocatalytic CO_2 reduction.

https://doi.org/10.1021/jacs.5c10614
J. Am. Chem. Soc. XXXX, XXX, XXX−XXX

Scheme 3. Reductive Quenching Processes of the Singlet and Triplet Excited States of 4DPAIPN by BIH and the Backward Electron Transfer of the Produced Geminate Ion Pairs

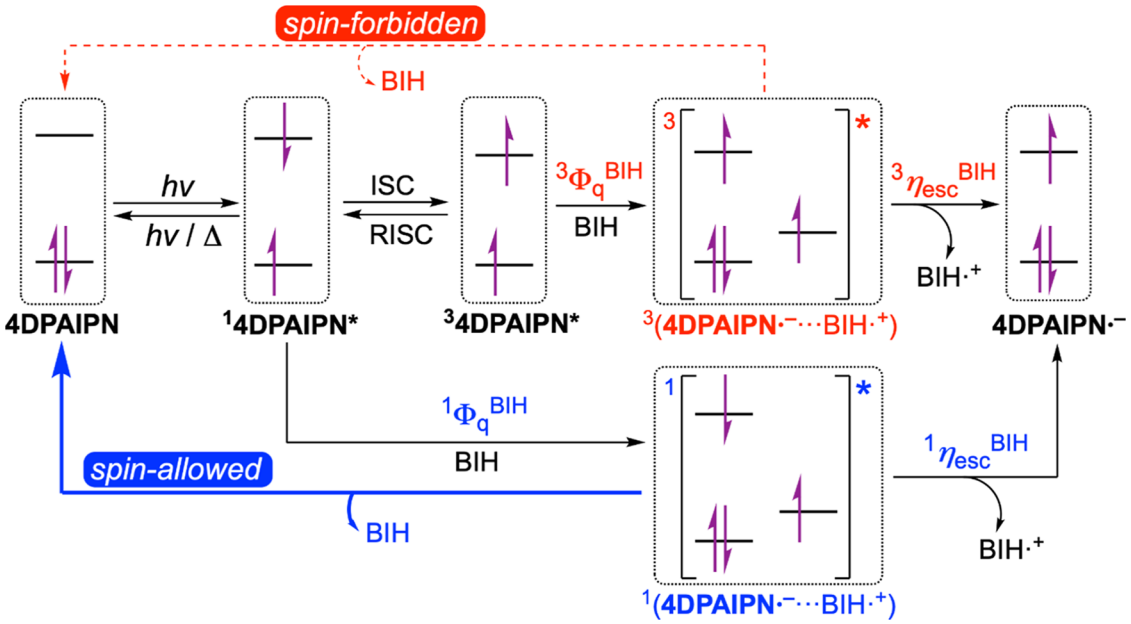

Scheme 4. Photochemical Two-Electron Oxidation of BIH by One-Photon Excitation of 4DPAIPN

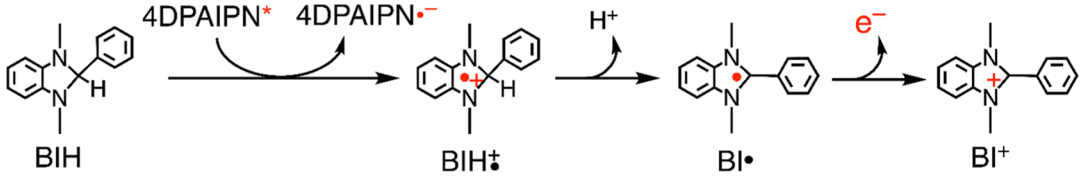

It was reported that rapid proton loss from BIH•+ to give BI•, which acts as another strong electron donor (E(BI+/BI•) = − 2.06 V vs Fc+/Fc[60])[61] capable of donating one electron to **Mn** and/or reaction intermediate(s) (Scheme 4). As the production of CO and $HCOO^-$ from CO_2 requires a two-electron reduction of **Mn** and BIH can donate two electrons to the catalytic cycle by one-photon excitation of **PS**, the quantum yield of photocatalytic CO_2 reduction can be expressed as eq 8, where $^1\eta_{esc}^{BIH}$ and $^3\eta_{esc}^{BIH}$ are the escape yields affording the free OERS of **4DPAIPN** (**4DPAIPN**•−) from ^{1}(**4DPAIPN**•−···$BIH^{•+}$) and ^{3}(**4DPAIPN**•−···$BIH^{•+}$), respectively. It should be reasonable because the selectivity and turnover number for CO_2 reduction are very high and the electron transfer from **4DPAIPN**•− to **Mn** should proceed efficiently due to the more negative reduction potential of **4DPAIPN** ($E_{1/2}^{red}$ = − 2.08 V vs Fc+/Fc) than **Mn** (E_p^{red} = − 1.83 V). It is noteworthy that the turnover number was very high ($TON_{CO+HCOO-}$ = 665). This means almost all of photochemically accumulated "electrons" (**4DPAIPN**•−, BI•) efficiently used for the photocatalytic CO_2 reduction. When, in addition, we measured the quantum yields $\Phi_{CO+HCOO-}$, we carefully selected a low light intensity for not accumulating **4DPAIPN**•− in the reaction solution.

$$\Phi_{CO+HCOO-} = 1/2 \times \{2 \times ({}^1\Phi_q^{BIH} \times {}^1\eta_{esc}^{BIH} + {}^3\Phi_q^{BIH} \times {}^3\eta_{esc}^{BIH})\}$$
$$= {}^1\Phi_q^{BIH} \times {}^1\eta_{esc}^{BIH} + {}^3\Phi_q^{BIH} \times {}^3\eta_{esc}^{BIH} \quad (8)$$

The escape yields were estimated as $^1\eta_{esc}^{BIH}$ = 0.063 and $^3\eta_{esc}^{BIH}$ = 0.53 based on eq 8, by using the observed $\Phi_{CO+HCOO-}$, and the calculated $^1\Phi_q^{BIH}$ and $^3\Phi_q^{BIH}$ by least-squares method, of which coefficient of determination was R^2 = 0.98. Consequently, the escape yield via reductive quenching of ^{3}**4DPAIPN*** was found to be 8.4 times more efficient than that of ^{1}**4DPAIPN*** for inducing the photocatalytic reaction.

$^1\eta_{esc}^{BIH}$ and $^3\eta_{esc}^{BIH}$ include the contributions of two different variables, namely (i) the escape yields from geminate ion pairs of (**4DPAIPN**•−···$BIH^{•+}$) to form free **4DPAIPN**•− ($^1\eta_{esc}'$ and $^3\eta_{esc}'$) and (ii) the fraction of **4DPAIPN**•− surviving the backward electron transfer induced by the recollision of the doublet free radicals of **4DPAIPN**•− and BIH•+ (η_{suv}), i.e., $^1\eta_{esc}^{BIH} = {}^1\eta_{esc}' \times \eta_{suv}$ and $^3\eta_{esc}^{BIH} = {}^3\eta_{esc}' \times \eta_{suv}$. Although $^1\eta_{esc}'$, $^3\eta_{esc}'$, and η_{suv} could not be individually determined based on the results of our experiments, previous studies on Class 1 photosensitizers reported that the survival ratio is negligible ($\eta_{suv} \sim 1$) compared with the escape yields from geminate ion pairs, probably because the concentrations of **4DPAIPN**•− and BIH•+ are extremely low under the employed conditions (no laser light) and proton loss from BIH•+ is very rapid.[40,41,61] Given that even if the survival ratio is smaller than unity (η_{suv} < 1), this value is not affected by the spin of the excited states, and the ratios of the escape yields ($^3\eta_{esc}^{BIH}/{}^1\eta_{esc}^{BIH}$ and $^3\eta_{esc}'/{}^1\eta_{esc}'$) should be the same, i.e., $^3\eta_{esc}^{BIH}/{}^1\eta_{esc}^{BIH} = ({}^3\eta_{esc}'\eta_{suv})/({}^1\eta_{esc}'\eta_{suv}) = {}^3\eta_{esc}'/{}^1\eta_{esc}'$.

Even though the singlet excited state was reductively quenched, 93.7% of ^{1}(**4DPAIPN**•−···$BIH^{•+}$) experienced backward electron transfer resulting in photon energy loss in

https://doi.org/10.1021/jacs.5c10614
J. Am. Chem. Soc. XXXX, XXX, XXX−XXX

Table 3. Quantum Yields (%) of CO_2 Reduction,[a] Reductive Quenching,[b] and One-Electron Reduction of 3DPAFIPN[c] at Various Concentrations of BIH for 3DPAFIPN as a PS

[BIH]/mM	Φ_{CO}	Φ_{HCOO-}	$\Phi_{CO+HCOO-}$	Φ_{OERS}	Φ_q^{total}[d]	${}^1\Phi_q^{BIH+TEOA}$	${}^3\Phi_q^{BIH+TEOA}$	${}^1\Phi_q^{BIH}$	${}^3\Phi_q^{BIH}$	${}^1\Phi_q^{TEOA}$	${}^3\Phi_q^{TEOA}$
0	3.6	4.6	8.2	20.1	76	50	26	0	0	50	26
10	3.6	8.3	11.9	23.8	79	56	23	12	2	44	21
100	1.8	5.4	7.2	12.3	90	79	11	58	5	21	6
200	1.0	3.1	4.1	6.2	94	87	7	74	4	13	3

[a]Quantum yields for CO_2 reduction: CO_2-saturated DMA solutions (4 mL) containing **3DPAFIPN** (250 μM), **Mn** (50 μM), BIH, and TEOA (1.5 M) were irradiated at λ_{ex} = 430 nm and light intensity = 5.0×10^{-9} Einstein·s^{-1}. [b]Calculated quantum yields for the reductive quenching of the singlet or triplet excited state of **3DPAFIPN** by BIH and/or TEOA (1.5 M). [c]Quantum yields for the one-electron reduction of **3DPAFIPN**: CO_2-saturated DMA solutions (4 mL) containing **3DPAFIPN** (0.1 mM), BIH, and TEOA (1.5 M) were irradiated at λ_{ex} = 436 nm and light intensity = (4.7−5.4)×10^{-9} Einstein·s^{-1}. [d]$\Phi_q^{total} = {}^1\Phi_q^{BIH+TEOA} + {}^3\Phi_q^{BIH+TEOA} = {}^1\Phi_q^{BIH} + {}^1\Phi_q^{TEOA} + {}^3\Phi_q^{BIH} + {}^3\Phi_q^{TEOA}$.

Table 4. Photophysical Properties and Photochemical-Process Rate Constants of 4DPAIPN and 3DPAFIPN

	Φ_{em}^{Ar}	Φ_{em}^{air}	τ_{PF} (ns)	τ_{TADF} (μs)	k_r (10^7 s^{-1})	k_{nr} (10^8 $M^{-1}s^{-1}$)	k_{ISC}	k_{RISC}	${}^1k_q^{BIH}$	${}^3k_q^{BIH}$	${}^1k_q^{TEOA}$	${}^3k_q^{TEOA}$
4DPAIPN	48.9	6.8	2.9	84	2.2	2.3	29	0.010	36	20	~0	0.00032
3DPAFIPN	17.5	8.2	3.6	43	2.3	11	15	0.0050	80	23	1.9	1.7

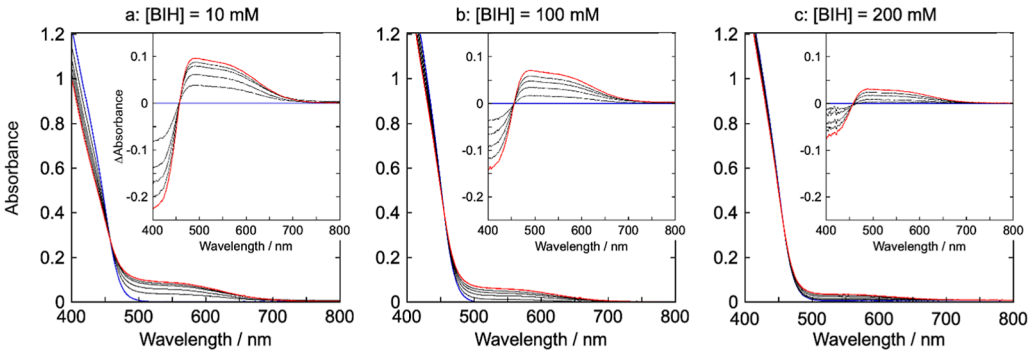

Figure 5. Changes in the UV−vis absorption spectrum of a CO_2-saturated DMA−TEOA (1.5 M) solution containing **3DPAFIPN** (0.1 mM) and BIH (a: 10 mM; b: 100 mM; c: 200 mM) during irradiation at 436 nm for 0−200 s at 40 s intervals. Insets display the corresponding difference spectra between post- and preirradiation spectra. Blue and red lines represent the spectra recorded at 0 and 200 s, respectively. Light intensity: (a) 5.4, (b) 5.2, and (c) 4.7×10^{-9} Einstein·s^{-1}.

the photocatalytic reactions. Therefore, to construct more efficient photocatalytic systems, conditions suppressing the reductive quenching of the singlet excited state of **PS** and favoring that of its triplet excited state should be established.

Although we tried to determine the quantum yields of OERS (**4DPAIPN•**$^-$) formation in the absence of **Mn** and CO_2 to obtain more direct evidence for the effect of the spin states of the geminate ion pair on the **4DPAIPN•**$^-$ formation yield (Figure S5), its spectral shape was substantially different from that of **4DPAIPN•**$^-$ obtained by flow electrolysis method (Figure S6) especially at λ < 480 nm region. It clearly indicates that side reactions of BI• proceed to the other products due to the more negative reduction potential of **4DPAIPN** ($E_{1/2}^{red}$ = − 2.08 vs Fc^+/Fc) than that of BI• ($E(BI^+/BI•)$ = − 2.06 V). This side reaction does not occur in the photocatalytic CO_2 reduction reaction because BI• provide an electron to **Mn** and/or reaction intermediate(s) of **Mn**, which is used for CO_2 reduction. Therefore, we used **3DPAFIPN** ($E_{1/2}^{red}$ = − 1.94 V) for this purpose (see next section).

2.2. Case Study of 3DPAFIPN. In the case of **3DPAFIPN** as the **PS**, the dependence of $\Phi_{CO+HCOO-}$ on the BIH concentration was similar to that observed for **4DPAIPN** (Table 3 and Figure S7), i.e., these variables were negatively correlated. The $\Phi_{CO+HCOO-}$ values observed for **3DPAFIPN** were notably lower than those observed for **4DPAIPN**. The differences between these two photocatalytic systems are discussed in detail in the subsequent section.

We determined the rates and quantum yields of the photophysical and quenching processes in the case of **3DPAFIPN** using the method employed in the case of **4DPAIPN** as follows.

(1) Based on the observed photophysical properties of **3DPAFIPN** as $\Phi_{PF} \approx \Phi_{em}^{air}$ = 8.2%, $\Phi_{TADF} \approx \Phi_{em}^{Ar} - \Phi_{em}^{air}$ = 17.5−8.2 = 9.3%, τ_{PF} = 3.6 ns, and τ_{TADF} = 43 μs, the rate constants of photophysical processes were determined as $k_r = 2.3 \times 10^7$ s^{-1}, $k_{nr} = 1.1 \times 10^8$ s^{-1}, $k_{ISC} = 1.5 \times 10^8$ s^{-1}, $k_{RISC} = 5.0 \times 10^4$ s^{-1}.

(2) The rate constants of reductive quenching were obtained using the Stern−Volmer analyses of emission lifetimes as ${}^1k_q^{BIH} = 8.0 \times 10^9$ $M^{-1}s^{-1}$, ${}^3k_q^{BIH} = 2.3 \times 10^9$ $M^{-1}s^{-1}$, ${}^1k_q^{TEOA} = 1.9 \times 10^8$ $M^{-1}s^{-1}$, and ${}^3k_q^{TEOA} = 1.7 \times 10^8$ $M^{-1}s^{-1}$ (Figures S8 and S9).

The results obtained for **3DPAFIPN** and **4DPAIPN** are summarized in Table 4 for comparison, and a detailed discussion is provided in the next section.

(3) Using the rate constants of the photophysical and photochemical processes and the method employed in the case of **4DPAIPN**, we also calculated the quantum yields of the reductive quenching of ^{1}**3DPAFIPN***

https://doi.org/10.1021/jacs.5c10614
J. Am. Chem. Soc. XXXX, XXX, XXX−XXX

^{3}**3DPAFIPN*** ($^1\Phi_q$ and $^3\Phi_q$) by BIH and TEOA (Table 3).

The reductive quenching of excited **3DPAFIPN** by TEOA was notably faster than that of excited **4DPAIPN** owing to the higher oxidizing power of the former (Table 1), which resulted in a substantial contribution of reductive quenching by TEOA to the photocatalytic reactions. Especially at lower BIH concentrations ([BIH] = 0−10 mM, [TEOA] = 1.5 M), both the singlet and triplet excited states were mainly quenched by TEOA, as the differences between the rate constants of reductive quenching by TEOA ($(1.7-1.9)\times10^8$ $M^{-1}s^{-1}$) and BIH ($(2.3-8.0)\times10^9$ $M^{-1}s^{-1}$) were smaller than the difference between the BIH and TEOA concentrations.

The quantum yields of **3DPAFIPN•$^-$** formation (Φ_{OERS}) were measured at various BIH concentrations. The irradiation of a DMA−TEOA (1.5 M) solution containing **3DPAFIPN** and BIH (without **Mn**) at 436 nm caused an absorption decrease at 400−450 nm and increase at 460−700 nm, with an isosbestic point at 457 nm (Figure 5). The spectral changes occurred more rapidly at lower BIH concentrations. The shapes of the difference spectra between before and after irradiation (insets in Figure 5) well agreed with that of **3DPAFIPN•$^-$** obtained by flow electrolysis (Figure 6), which

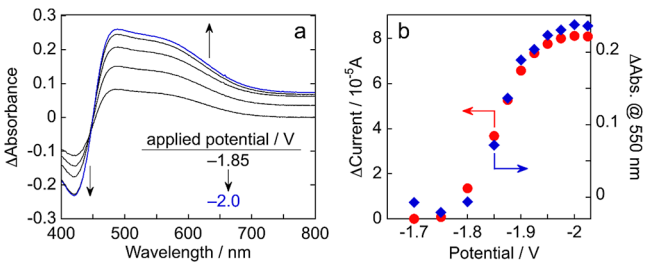

Figure 6. (a) Changes in the UV−vis absorption spectrum of an Ar-saturated DMA solution containing **3DPAFIPN** (0.5 mM) and Et_4NBF_4 (0.1 M) during flow electrolysis at applied potentials between −1.85 and −2.0 V. (b) Current (●) and absorbance at 550 nm (◆) as functions of the applied potential.

indicated that during photoirradiation in the presence of BIH and TEOA, **3DPAFIPN** was reduced to **3DPAFIPN•$^-$**. Time conversion of **3DPAFIPN** to **3DPAFIPN•$^-$** in the photochemical reactions as a function of the number of absorbed photons was plotted (Figure 7) using the molecular extinction

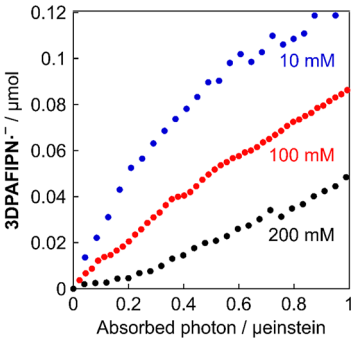

Figure 7. Photochemical production of **3DPAFIPN•$^-$** as a function of the number of absorbed photons. A CO_2-saturated DMA−TEOA (1.5 M) solution containing **3DPAFIPN** (0.1 mM) and BIH (blue plots: 10 mM; red plots: 100 mM; black plots: 200 mM) was irradiated at 436 nm.

coefficient of **3DPAFIPN•$^-$** (ε_{550nm} = 3.2 × 10^3 $M^{-1}cm^{-1}$) obtained by flow electrolysis; these curves were used to determine the quantum yields of **3DPAFIPN•$^-$** (Table 3).

Φ_{OERS} was negatively correlated with the concentration of BIH (Figure 8), and the Φ_{OERS} values were similar to the

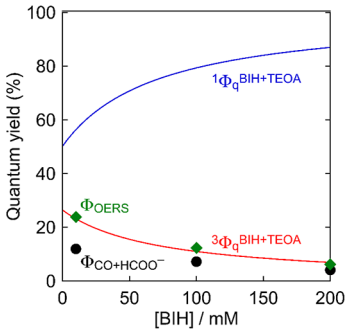

Figure 8. Observed quantum yields for CO_2 reduction using **3DPAFIPN** as a redox photosensitizer (●) and formation of **3DPAFIPN•$^-$** (◆), and calculated quantum yields for the reductive quenching from singlet ($^1\Phi_q^{BIH+TEOA}$, blue line) or triplet ($^3\Phi_q^{BIH+TEOA}$, red line) excited states of **3DPAFIPN** by BIH and TEOA (1.5 M) as functions of the BIH concentration.

duplicated values of $^3\Phi_q^{BIH+TEOA}$ (Table 3). This behavior strongly suggests that the quenching of ^{3}**3DPAFIPN*** efficiently supplies **3DPAFIPN•$^-$**, whereas that of ^{1}**3DPAFIPN*** does not. The similar dependences of $\Phi_{CO+HCOO-}$ and Φ_{OERS} on the BIH concentration suggest that the reductive quenching of the triplet excited state substantially contributes not only to the one-electron reduction of **3DPAFIPN** but also to photocatalysis. The Φ_{OERS} values were approximately two times larger than the $\Phi_{CO+HCOO-}$ values (Table 3 and Figure 8), which is reasonable, as the reduction of CO_2 to CO or $HCOO^-$ requires two electrons.

The excited states of **3DPAFIPN** were quenched by TEOA in the absence of BIH. Therefore, we determined the quantum yields of the reductive quenching of the excited states by TEOA and formation of **3DPAFIPN•$^-$** in the absence of BIH and presence of different concentrations of TEOA (33.5 mM, 1.5 M) (Table 5; Figures S10 and S11). Using these data and Φ_{OERS}s instead of $\Phi_{CO+HCOO-}$ and the similar method applied in the case of **4DPAIPN** (see Supporting Information for detail), we determined the escape yields for the production of free **3DPAFIPN•$^-$** from ^{1}(**3DPAIPN•$^-$**···TEOA$^{\bullet+}$) and

Table 5. Quantum Yields (%) for CO_2 Reduction[a], 3DPAFIPN$^{\cdot-}$ Production[b], and the Reductive Quenching of the Excited States of 3DPAFIPN by TEOA[c]

[TEOA]/M	Φ_{CO}	Φ_{HCOO-}	$\Phi_{CO+HCOO-}$	Φ_{OERS}	$^1\Phi_q^{TEOA}$	$^3\Phi_q^{TEOA}$
0.0335	−[d]	−[d]	−[d]	43.2	2	52
1.5	3.6	4.6	8.2	20.1	50	26

[a]Quantum yields for CO_2 reduction: CO_2-saturated DMA solutions (4 mL) containing **3DPAFIPN** (250 μM), **Mn** (50 μM), and TEOA (1.5 M) were irradiated at λ_{ex} = 430 nm and light intensity = 5.0 × 10^{-9} Einstein·s^{-1}. [b]Quantum yields of the one-electron reduction of **3DPAFIPN**: CO_2-saturated DMA solutions (4 mL) containing **3DPAFIPN** (0.1 mM) and TEOA were irradiated at 436 nm (intensity = 1.0 × 10^{-8} Einstein·s^{-1}). [c]Calculated quantum yields of the reductive quenching of the singlet or triplet excited states of **3DPAFIPN** by TEOA. [d]Very low product yield.

https://doi.org/10.1021/jacs.5c10614
J. Am. Chem. Soc. XXXX, XXX, XXX−XXX

^{3}(**3DPAIPN**$\bullet^-$···TEOA$^{\bullet+}$) as $^1\eta_{esc}^{TEOA} \approx 0$ and $^3\eta_{esc}^{TEOA} = 0.41$. By adding these data to the analysis of the reductive quenching of the excited states of **3DPAFIPN** by BIH, we determined the escape yields for the production of free **3DPAFIPN**$\bullet^-$ from ^{1}(**3DPAIPN**$\bullet^-$···BIH$^{\bullet+}$) and ^{3}(**3DPAIPN**$\bullet^-$···BIH$^{\bullet+}$) as $^1\eta_{esc}^{BIH} \approx 0$ and $^3\eta_{esc}^{BIH} = 0.69$. Notably, the $^3\eta_{esc}^{BIH}$ of **3DPAIPN** exceeded that of **4DPAIPN** ($^3\eta_{esc}^{BIH} = 0.53$). The origin of difference is discussed in the next section. Using these estimated escape yields, we simulated the quantum yields for CO_2 reduction ($^{SIM}\Phi_{CO+HCOO-}$) and found good agreement with the measured $\Phi_{CO+HCOO-}$ values (Table 6). These results support the appropriateness of the escape yield estimation in the **4DPAIPN** system using $\Phi_{CO+HCOO-}$ instead of Φ_{OERS} (eq 8).

Table 6. Comparison Between the Simulated and Measured $\Phi_{CO+HCOO-}$ in the 3DPAFIPN System

[BIH]/mM	$\Phi_{CO+HCOO-}$	$^{SIM}\Phi_{CO+HCOO-}$[a]
10	11.9	10.0
100	7.2	6.0
200	4.1	4.1

[a] $^{SIM}\Phi_{CO+HCOO-} = 1/2 \times 2\times(^1\Phi_q^{BIH} \times {}^1\eta_{esc}^{BIH} + {}^3\Phi_q^{BIH} \times {}^3\eta_{esc}^{BIH} + {}^1\Phi_q^{TEOA} \times {}^1\eta_{esc}^{TEOA} + {}^3\Phi_q^{TEOA} \times {}^3\eta_{esc}^{TEOA}) = {}^1\Phi_q^{BIH} \times {}^1\eta_{esc}^{BIH} + {}^3\Phi_q^{BIH} \times {}^3\eta_{esc}^{BIH} + {}^1\Phi_q^{TEOA} \times {}^1\eta_{esc}^{TEOA} + {}^3\Phi_q^{TEOA} \times {}^3\eta_{esc}^{TEOA}$.

In the presence of only TEOA as a reductant (that is, in the absence of BIH), low TEOA concentrations can photochemically produce **3DPAIPN**$\bullet^-$ in a higher yield (Table 5). On the other hand, when the photocatalytic reaction was conducted at a low concentration of TEOA (33.5 mM), the amounts of the produced CO and $HCOO^-$ were markedly smaller than those observed for 1.5 M TEOA. It was reported that catalytic CO_2 reduction by Mn complexes requires a proton source such as TEOA, water, or PhOH.[62,63] Thus, the TEOA concentration of 33.5 mM should not be enough for efficient photocatalysis for CO_2 reduction in the system using **Mn** as the catalyst.

2.3. Comparison of 3DPAFIPN and 4DPAIPN as PSs.

Table 3 and Figure 8 summarize the quantum yields of the reductive quenching of the singlet ($^1\Phi_q^{BIH+TEOA}$) and triplet ($^3\Phi_q^{BIH+TEOA}$) excited states of **3DPAFIPN** by BIH (at various concentrations) and TEOA (1.5 M), along with the quantum yields of CO_2 reduction. For the photocatalytic reactions with **3DPAFIPN** as the **PS**, the dependence of the quantum yield of CO_2 reduction on the concentration of BIH was similar to that observed for **4DPAIPN** (Table 2 and Figure 4), that is, these parameters were negatively correlated.

At every concentration of BIH, in the case of **3DPAFIPN** as the **PS**, $\Phi_{CO+HCOO-}$ was markedly lower than that observed for **4DPAIPN** (for example, at [BIH] = 10 mM, 11.9% (**3DPAFIPN**) vs 42.2% (**4DPAIPN**)). The $^3\Phi_q^{BIH+TEOA}$ of **3DPAFIPN** was also lower (23% at [BIH] = 10 mM, for example) than that observed for **4DPAIPN** ($^3\Phi_q^{BIH}$ = 78%) at every concentration owing to the quenching of ^{1}**3DPAFIPN*** ($^1\Phi_q^{BIH+TEOA}$ = 56%) by BIH and TEOA being more efficient than that of ^{1}**4DPAIPN*** by BIH ($^1\Phi_q^{BIH}$ < 10%, ^{1}**4DPAIPN*** was quenched by BIH but not TEOA). As summarized in Table 7, the ratios of $^3\Phi_q^{BIH+TEOA}$ between **3DPAFIPN** and **4DPAIPN** were similar to the ratios of $\Phi_{CO+HCOO-}$ between **3DPAFIPN** and **4DPAIPN**. Therefore, we can conclude that the lower photocatalytic activity of the system with **3DPAFIPN** was mainly caused by the higher quantum yield of ^{1}**3DPAFIPN*** quenching by BIH and TEOA, which causes lower $^3\Phi_q^{BIH+TEOA}$.

Table 7. Comparison Between 3DPAFIPN and 4DPAIPN[a]

[BIH]/mM	ratio of $^3\Phi_q^{BIH+TEOA}$[b] 3DPAFIPN/4DPAIPN	ratio of $\Phi_{CO+HCOO-}$ 3DPAFIPN/4DPAIPN
10	29:100	28:100
100	26:100	32:100
200	25:100	20:100

[a] Each data of $^3\Phi_q^{BIH+TEOA}$ and $\Phi_{CO+HCOO-}$ is shown in Tables 2 and 3. [b] In the case of **4DPAIPN**, $^3\Phi_q^{BIH+TEOA}$ is $^3\Phi_q^{BIH}$ shown in Table 2 because quenching by TEOA is negligible. See the main text.

We rationalized the more efficient quenching of ^{1}**3DPAFIPN*** compared with that of ^{1}**4DPAIPN*** using photophysical (Table 3) and electrochemical (Table 1) property analyses. The τ_{PF} of ^{1}**3DPAFIPN*** (3.6 ns) was not particularly different from that of ^{1}**4DPAIPN*** (2.9 ns). Therefore, the difference in the lifetimes of the singlet excited states produced just after excitation should not be the main factor affecting $\Phi_{CO+HCOO-}$. Conversely, the difference in the reduction potentials of the singlet excited states, i.e., $E(^1$**3DPAFIPN***/**3DPAFIPN**$\bullet^-) = +0.74$ V vs Fc^+/Fc and $E(^1$**4DPAIPN***/**4DPAIPN**$\bullet^-) = +0.51$ V, was concluded to strongly influence $\Phi_{CO+HCOO-}$. The quenching of ^{1}**3DPAFIPN*** by BIH was 2.2 times faster than that of ^{1}**4DPAIPN*** because of the higher oxidizing power of the former. The weaker reductant TEOA quenched ^{1}**3DPAFIPN*** but not ^{1}**4DPAIPN***. The quenching rates at [BIH] = 10 mM were determined as follows.

$$^1\textbf{3DPAFIPN}^*: {}^1k_q^{BIH}[BIH] + {}^1k_q^{TEOA}[TEOA] = 80 \times 10^8 \times 0.01 + 1.9 \times 10^8 \times 1.5 = 3.65 \times 10^8\ s^{-1} \quad (9)$$

$$^1\textbf{4DPAIPN}^*: {}^1k_q^{BIH}[BIH] + {}^1k_q^{TEOA}[TEOA] = 36 \times 10^8 \times 0.01 + 0 \times 1.5 = 0.36 \times 10^8\ s^{-1} \quad (10)$$

This one-order difference resulted in the formation yield of the triplet excited state ^{3}**3DPAFIPN*** being lower than that of ^{3}**4DPAIPN***, which was the main reason for why photocatalysis with **3DPAFIPN** as the **PS** was markedly less efficient than that observed for **4DPAIPN** because the triplet states of both **PS**s were almost quantitatively quenched even in the presence of low concentrations of BIH (e.g., 10 mM), with the quenching of the triplet excited state resulting in a markedly higher formation quantum yield of the one-electron-reduced **PS**.

The excited-state properties should also affect photocatalysis. Formation quantum yields of ^{3}**3DPAFIPN*** and ^{3}**4DPAIPN*** in the absence of quenchers, which are the quantum yields of the intersystem crossing from the corresponding singlet excited states (Φ_{ISC}), can be obtained by using eq 11.

$$\Phi_{ISC} = k_{ISC}/(k_r + k_{nr} + k_{ISC}) = \Phi_{TADF}/(\Phi_{PF} + \Phi_{TADF}) \approx (\Phi_{em}^{Ar} - \Phi_{em}^{air})/\Phi_{em}^{Ar} \quad (11)$$

https://doi.org/10.1021/jacs.5c10614
J. Am. Chem. Soc. XXXX, XXX, XXX−XXX

Even in the case of ideal reductive quenching, that is, no quenching of the singlet excited state and the complete quenching of the triplet excited state, the maximum ${}^3\Phi_q$ of **3DPAFIPN**, equaling to Φ_{ISC}, was estimated as ${}^3\Phi_q{}^{max} = 53\%$. This value is substantially smaller than that of **4DPAIPN** (${}^3\Phi_q{}^{max} = 86\%$). The higher ${}^3\Phi_q{}^{max}$ (i.e., Φ_{ISC}) of **4DPAIPN** is caused by the 4.8-times slower k_{nr} and 1.9-times faster k_{ISC} of **4DPAIPN** compared with those of **3DPAFIPN** (their k_rs were similar). That is, the ratio of emission quenching by O_2 in air should be a useful indicator for estimating the usefulness of TADF molecules as **PS**s when TADF can be almost quantitatively quenched by O_2, as in the cases of **4DPAIPN** and **3DPAFIPN**.

The abundance ratio of the triplet excited state and reaction conditions minimizing electron transfer from the singlet excited state, as well as the UV−vis absorptive properties and redox potentials, are highly important for the construction of efficient photocatalytic systems using TADF-type organic photosensitizers. This is a unique feature of purely organic photosensitizers, as metal-complex-based photosensitizers usually quantitatively form triplet excited states.

Finally, we examined the dependence of the free energy of electron transfer from BIH/TEOA to ^{3}**PS*** on the escape yields to produce the free OERS of **PS**s, as in the case of heavy-transition-metal complexes (Class 1 **PS**s), the higher free-energy changes of photoinduced electron transfer result in higher quantum yields of the free OERS of **PS**s (Φ_{OERS}) owing to the larger distance between the produced radical ions in the geminate ion pair.[40,41] The free-energy changes of the photoinduced electron transfer followed the order of [^{3}**3DPAFIPN***, BIH] (0.64 eV) > [^{3}**4DPAIPN**, BIH] (0.45 eV) > [^{3}**3DPAFIPN***, TEOA] (0.09−0.34 eV), and the yields of the free OERS of **PS**s followed the order of ^{3}(**3DPAFIPN**$\bullet^-\cdots$BIH$^{\bullet+}$) (${}^3\eta_{esc}{}^{BIH} = 0.69$) > ^{3}(**4DPAIPN**$\bullet^-\cdots$BIH$^{\bullet+}$) (${}^3\eta_{esc}{}^{BIH} = 0.53$) > ^{3}(**3DPAFIPN**$\bullet^-\cdots$TEOA$^{\bullet+}$) (${}^3\eta_{esc}{}^{TEOA} = 0.41$). Therefore, in the case of TADF **PS**s as well, the larger free-energy changes of photoinduced electron transfer probably favored the formation of the OERS of **PS**s. This behavior frequently increases the efficiency of the photocatalytic reaction owing to the larger distance between the radical ions in the geminate ion pair.

3. CONCLUSION

Redox photosensitization processes using purely organic compounds displaying TADF were minutely investigated, focusing on the spin state of their excited states. Given that two different excited states, that is, the lowest singlet and triplet excited states, are thermally equilibrated with different lifetimes in the case of TADF-type molecules, unlike in the case of the frequently used photosensitizers such as Ru(II) and Ir(III) complexes, both these excited states can contribute to photoinduced electron transfer processes. Therefore, we investigated the characteristics and roles of the singlet and triplet excited states in photocatalytic CO_2 reduction as a typical redox-photosensitized reaction. Two organic compounds exhibiting TADF, **4DPAIPN** and **3DPAFIPN**, were used as **PS**s in combination with a manganese(I) complex as a catalyst and BIH and TEOA as sacrificial electron donors. In the case of **4DPAIPN**, the quantum yield of CO_2 reduction ($\Phi_{CO+HCOO-}$) was negatively correlated with the concentration of BIH, with the maximal value of 43.2% achieved at [BIH] = 5 mM (cf. $\Phi_{CO+HCOO-}$ = 20.3% at [BIH] = 200 mM). The reason for this unusual dependence of $\Phi_{CO+HCOO-}$ on the BIH concentration was the difference in the reductive quenching processes between the singlet and triplet excited states. The reduction of the singlet excited state by BIH afforded a singlet geminate ion pair, ^{1}(**4DPAIPN**$\bullet^-\cdots$BIH$^{\bullet+}$), which experienced a notably faster backward electron transfer to the ground state than the triplet geminate ion pair formed by the reduction of the triplet excited state, ^{3}(**4DPAIPN**$\bullet^-\cdots$BIH$^{\bullet+}$). The escape yields of the singlet and triplet geminate ion pairs producing OERS were estimated as ${}^1\eta_{esc}{}^{BIH} = 0.063$ and ${}^3\eta_{esc}{}^{BIH} = 0.53$, respectively, in the case of **4DPAIPN**. That is, at higher BIH concentrations, the singlet excited state was quenched to a larger extent, which resulted in less formation of the triplet excited state and a lower photocatalytic efficiency. The **3DPAFIPN** system exhibited a similar tendency, with the maximum $\Phi_{CO+HCOO-}$ equaling only 11.9% at [BIH] = 10 mM. The difference between the photocatalytic systems with **4DPAIPN** and **3DPAFIPN** was ascribed to the higher oxidizing power of the latter, which induced the efficient quenching of the singlet excited state (^{1}**3DPAFIPN***) by TEOA, and the lower formation quantum yield of ^{3}**3DPAFIPN*** due to faster nonradiative decay and slower intersystem crossing from ^{1}**3DPAFIPN***.

These results help establishing suitable reaction conditions and molecular design rules for the construction of efficient photocatalytic systems using TADF-type photosensitizers. The reaction conditions should be optimized to minimize the inefficient quenching of the singlet excited state and maximize the quenching of the triplet excited state, e.g., by adjusting the quencher type and concentration. TADF molecules with a larger abundance ratio of the triplet excited state, which can be roughly estimated based on the results of emission quenching by O_2, are suitable **PS**s. This factor, along with visible light absorption, long-lived excited states, and appropriate redox potentials, is important for designing superior TADF photosensitizers.

4. EXPERIMENTAL SECTION

4.1. Photophysical Measurements. UV−vis absorption spectra were recorded using a JASCO V-670 spectrophotometer. Emission spectra were recorded using a HORIBA Fluorolog-3−21 spectrofluorometer equipped with an NIR-PMT R5509−43 near-infrared detector. Emission lifetimes were determined using a HORIBA Jobin-Yvon FluoroCube time-correlated single-photon counting system. Prior to emission measurements, the sample solutions were degassed for 20 min under Ar. Emission-quenching experiments were performed in Ar-saturated or air-equilibrated solutions containing an organic photosensitizer and BIH/TEOA.

4.2. Photocatalytic Reactions. Photocatalytic reactions were performed in a DMA−TEOA (1.5 M) solution containing the organic photosensitizer (50 μM or 250 μM), **Mn** (50 μM), and BIH. The solution (4 mL) was purged with CO_2 for 20 min in a quartz cubic cell (11 mL, light path length: 10 mm) and then irradiated using a Shimadzu QYM-01 photoreaction quantum yield evaluation system equipped with a 300 W xenon lamp and band-pass filter or a Shimadzu Lightway (PQY-01) photoreaction evaluation system equipped with a LED light source. The solution was kept at 25 °C using an EYELA NCB-1210 constant-temperature system. Gaseous products (CO and H_2) were quantified using GC-TCD (GL Science GC323). $HCOO^-$ was quantified using capillary electrophoresis (Agilent Technology 7100L).

4.3. Photochemical Formation of the OERS of 3DPAFIPN. A CO_2-saturated DMA−TEOA (1.5 M) solution containing **3DPAFIPN** (0.1 mM) and BIH in a quartz cubic cell (light pass length: 10 mm) was irradiated using a 500 W xenon lamp with a band-pass filter. Changes in the UV−vis absorption spectrum during irradiation were measured using a photodiode array spectrometer (Otsuka Electronics

https://doi.org/10.1021/jacs.5c10614
J. Am. Chem. Soc. XXXX, XXX, XXX−XXX

MCPD-9800). The solution was maintained at 25 °C using an EYELA NCB-1210 constant-temperature system.

4.4. Flow Electrolysis. UV−vis absorption spectra were recorded under bulk electrolysis conditions using a flow electrolysis apparatus. The applied potential was controlled using an ALS/CHI 760E electrochemical analyzer, and the spectra were monitored using a photodiode array spectrometer (Otsuka Electronics MCPD-9800). A DMA solution of the organic photosensitizer (0.5 mM) and Et_4NBF_4 (0.1 M) as a supporting electrolyte was purged with Ar for 40 min before measurements. The sample solution was transferred to a VF-2 electrolysis cell (EC Frontier) and then a quartz flow cell (light path length: 1.5 mm) at flow rate of 0.1 mL·min^{-1} using a JASCO PU-4180i pump. The flow electrolysis cell was constructed with a carbon-felt working electrode, $Ag/AgNO_3$ (10 mM) reference electrode, and Pt wire counter electrode. The number of electrons (n_e) consumed to reduce the organic photosensitizer was evaluated using eq 12. The reduction current (i) was calculated from the plateau of the current against the applied potential plots of the solution. The background current (i_0) was obtained from the plots of the electrolyte solution without an organic photosensitizer.

$$n_e = (i - i_0)/cvF \tag{12}$$

where F, c, and v are the Faraday constant, concentration of the organic photosensitizer, and flow rate, respectively.

4.5. Materials. DMA was dried over molecular sieves 4A and distilled under reduced pressure (∼10 mmHg). TEOA was distilled under reduced pressure (<1 mmHg). Et_4NBF_4 was recrystallized twice from acetonitrile/ethyl acetate and dried in vacuo at 100 °C overnight shortly before use. All other reagents were used as received without further purification. **4DPAIPN**,[53] **3DPAFIPN**,[22] **Mn**,[53] and BIH[60,64] were prepared as described in literature.

■ ASSOCIATED CONTENT

Supporting Information

The Supporting Information is available free of charge at https://pubs.acs.org/doi/10.1021/jacs.5c10614.

Cyclic voltammograms, Stern−Volmer plots from emission intensity decays, plots of photocatalytic CO_2 reduction, Emission quenching spectra, UV−vis absorption spectrum changes during irradiation, plot of quantum yields for reductive quenching and OERS formation of **3DPAFIPN**, kinetic analysis, and calculation of escape yields (PDF)

■ AUTHOR INFORMATION

Corresponding Authors

Yusuke Tamaki − *National Institute of Advanced Industrial Science and Technology (AIST), Sendai, Miyagi 983-8551, Japan*; orcid.org/0000-0003-4432-0025; Email: tamaki-y@aist.go.jp

Osamu Ishitani − *Department of Chemistry, Graduate School of Advanced Science and Engineering, Hiroshima University, Higashi-Hiroshima, Hiroshima 739-8526, Japan*; orcid.org/0000-0001-9557-7854; Email: iosamu@hiroshima-u.ac.jp

Authors

Kei Kamogawa − *Department of Chemistry, Graduate School of Advanced Science and Engineering, Hiroshima University, Higashi-Hiroshima, Hiroshima 739-8526, Japan*; orcid.org/0009-0004-7493-1999

Rei Inoue − *Department of Chemistry, School of Science, Tokyo Institute of Technology, Meguroku, Tokyo 152-8550, Japan*

Paola Ceroni − *Dipartimento di Chimica "Giacomo Ciamician", Alma Mater Studiorum− Universita di Bologna, 40126 Bologna, Italy*; orcid.org/0000-0001-8916-1473

Complete contact information is available at: https://pubs.acs.org/10.1021/jacs.5c10614

Notes

The authors declare no competing financial interest.

■ ACKNOWLEDGMENTS

We thank the Iwatani Naoji Foundation and JSPS (KAKENHI Grant Number: 22K19081) for the financial supports. Y.T. thanks JSPS (KAKENHI Grant Number: 24K08376).

■ REFERENCES

(1) Fukuzumi, S.; Jung, J.; Yamada, Y.; Kojima, T.; Nam, W. Homogeneous and Heterogeneous Photocatalytic Water Oxidation by Persulfate. *Chem. —Asian. J.* **2016**, *11*, 1138−1150.

(2) Yamazaki, Y.; Takeda, H.; Ishitani, O. Photocatalytic reduction of CO_2 using metal complexes. *J. Photochem. Photobiol. C* **2015**, *25*, 106−137.

(3) Prier, C. K.; Rankic, D. A.; MacMillan, D. W. C. Visible Light Photoredox Catalysis with Transition Metal Complexes: Applications in Organic Synthesis. *Chem. Rev.* **2013**, *113*, 5322−5363.

(4) Sakakibara, Y.; Murakami, K. Switchable Divergent Synthesis Using Photocatalysis. *ACS Catal.* **2022**, *12*, 1857−1878.

(5) Thompson, D. W.; Ito, A.; Meyer, T. J. $[Ru(bpy)_3]^{2+*}$ and other remarkable metal-to-ligand charge transfer (MLCT) excited states. *Pure Appl. Chem.* **2013**, *85*, 1257−1305.

(6) Juris, A.; Balzani, V.; Barigelletti, F.; Campagna, S.; Belser, P.; von Zelewsky, A. Ru(II) polypyridine complexes: photophysics, photochemistry, electrochemistry, and chemiluminescence. *Coord. Chem. Rev.* **1988**, *84*, 85−277.

(7) Pac, C.; Ihama, M.; Yasuda, M.; Miyauchi, Y.; Sakurai, H. Tris(2,2'-bipyridine)ruthenium(2+)-mediated photoreduction of olefins with 1-benzyl-1,4-dihydronicotinamide: a mechanistic probe for electron-transfer reactions of NAD(P)H-model compounds. *J. Am. Chem. Soc.* **1981**, *103*, 6495−6497.

(8) Ishida, H.; Terada, T.; Tanaka, K.; Tanaka, T. Photochemical CO2 Reduction Catalyzed by $[Ru(bpy)_2(CO)_2]^{2+}$ Using Triethanolamine and 1-Benzyl-1,4-dihydronicotinamide as an Electron Donor. *Inorg. Chem.* **1990**, *29*, 905−911.

(9) Ishizuka, T.; Hosokawa, A.; Kawanishi, T.; Kotani, H.; Zhi, Y.; Kojima, T. Self-Photosensitizing Dinuclear Ruthenium Catalyst for CO_2 Reduction to CO. *J. Am. Chem. Soc.* **2023**, *145*, 23196−23204.

(10) Zhu, M.; Zheng, N. Photoinduced Cleavage of N-N Bonds of Aromatic Hydrazines and Hydrazides by Visible Light. *Synthesis* **2011**, *2011*, 2223−2236.

(11) Larraufie, M. H.; Pellet, R.; Fensterbank, L.; Goddard, J. P.; Lacote, E.; Malacria, M.; Ollivier, C. Visible-light-induced photoreductive generation of radicals from epoxides and aziridines. *Angew. Chem., Int. Ed.* **2011**, *50*, 4463−4466.

(12) Hasegawa, E.; Takizawa, S.; Seida, T.; Yamaguchi, A.; Yamaguchi, N.; Chiba, N.; Takahashi, T.; Ikeda, H.; Akiyama, K. Photoinduced electron-transfer systems consisting of electron-donating pyrenes or anthracenes and benzimidazolines for reductive transformation of carbonyl compounds. *Tetrahedron* **2006**, *62*, 6581−6588.

(13) Tamaki, Y.; Koike, K.; Morimoto, T.; Yamazaki, Y.; Ishitani, O. Red-Light-Driven Photocatalytic Reduction of CO_2 using Os(II)-Re(I) Supramolecular Complexes. *Inorg. Chem.* **2013**, *52*, 11902−11909.

(14) Irikura, M.; Tamaki, Y.; Ishitani, O. Development of a panchromatic photosensitizer and its application to photocatalytic CO_2 reduction. *Chem. Sci.* **2021**, *12*, 13888−13896.

(15) Ravetz, B. D.; Tay, N. E. S.; Joe, C. L.; Sezen-Edmonds, M.; Schmidt, M. A.; Tan, Y.; Janey, J. M.; Eastgate, M. D.; Rovis, T.

Development of a Platform for Near-Infrared Photoredox Catalysis. *ACS Cent. Sci.* **2020**, *6*, 2053−2059.
(16) Takizawa, S.; Ikuta, N.; Zeng, F.; Komaru, S.; Sebata, S.; Murata, S. Impact of Substituents on Excited-State and Photosensitizing Properties in Cationic Iridium(III) Complexes with Ligands of Coumarin 6. *Inorg. Chem.* **2016**, *55*, 8723−8735.
(17) Kuramochi, Y.; Ishitani, O. Iridium(III) 1-Phenylisoquinoline Complexes as a Photosensitizer for Photocatalytic CO_2 Reduction: A Mixed System with a Re(I) Catalyst and a Supramolecular Photocatalyst. *Inorg. Chem.* **2016**, *55*, 5702−5709.
(18) Rao, H.; Schmidt, L. C.; Bonin, J.; Robert, M. Visible-light-driven methane formation from CO_2 with a molecular iron catalyst. *Nature* **2017**, *548*, 74−77.
(19) Morimoto, T.; Nishiura, C.; Tanaka, M.; Rohacova, J.; Nakagawa, Y.; Funada, Y.; Koike, K.; Yamamoto, Y.; Shishido, S.; Kojima, T.; Saeki, T.; Ozeki, T.; Ishitani, O. Ring-Shaped Re(I) Multinuclear Complexes with Unique Photofunctional Properties. *J. Am. Chem. Soc.* **2013**, *135*, 13266−13269.
(20) Takeda, H.; Koike, K.; Inoue, H.; Ishitani, O. Development of an Efficient Photocatalytic System for CO_2 Reduction Using Rhenium(I) Complexes Based on Mechanistic Studies. *J. Am. Chem. Soc.* **2008**, *130*, 2023−2031.
(21) Bryden, M. A.; Zysman-Colman, E. Organic thermally activated delayed fluorescence (TADF) compounds used in photocatalysis. *Chem. Soc. Rev.* **2021**, *50*, 7587−7680.
(22) Speckmeier, E.; Fischer, T. G.; Zeitler, K. A Toolbox Approach To Construct Broadly Applicable Metal-Free Catalysts for Photoredox Chemistry: Deliberate Tuning of Redox Potentials and Importance of Halogens in Donor-Acceptor Cyanoarenes. *J. Am. Chem. Soc.* **2018**, *140*, 15353−15365.
(23) Bonin, J.; Robert, M.; Routier, M. Selective and Efficient Photocatalytic CO_2 Reduction to CO Using Visible Light and an Iron-Based Homogeneous Catalyst. *J. Am. Chem. Soc.* **2014**, *136*, 16768−16771.
(24) Matsuoka, S.; Kohzuki, T.; Pac, C.; Ishida, A.; Takamuku, S.; Kusaba, M.; Nakashima, N.; Yanagida, S. Photocatalysis of Ollgo(*p*-phenylenes). Photochemical Reduction of Carbon Dloxlde with Trlethylamine. *J. Phys. Chem.* **1992**, *96*, 4437−4442.
(25) Ogata, T.; Yanagida, S.; Brunschwig, B. S.; Fujita, E. Mechanistic and Kinetic Studies of Cobalt Macrocycles in a Photochemical CO_2 Reduction System: Evidence of Co-CO_2 Adducts as Intermediates. *J. Am. Chem. Soc.* **1995**, *117*, 6708−6716.
(26) Guo, Z.; Cheng, S.; Cometto, C.; Anxolabéhère-Mallart, E.; Ng, S.-M.; Ko, C.-C.; Liu, G.; Chen, L.; Robert, M.; Lau, T.-C. Highly Efficient and Selective Photocatalytic CO2 Reduction by Iron and Cobalt Quaterpyridine Complexes. *J. Am. Chem. Soc.* **2016**, *138*, 9413−9416.
(27) Rao, H.; Bonin, J.; Robert, M. Visible-light Homogeneous Photocatalytic Conversion of CO_2 into CO in Aqueous Solutions with an Iron Catalyst. *ChemSusChem* **2017**, *10*, 4447−4450.
(28) Ogata, T.; Yamamoto, Y.; Wada, Y.; Murakoshi, K.; Kusaba, M.; Nakashima, N.; Ishida, A.; Takamuku, S.; Yanagida, S. Phenazine-Photosensitized Reduction of CO_2 Mediated by a Cobalt-Cyclam Complex through Electron and Hydrogen Transfer. *J. Phys. Chem.* **1995**, *99*, 11916−11922.
(29) Rao, H.; Lim, C.-H.; Bonin, J.; Miyake, G. M.; Robert, M. Visible-Light-Driven Conversion of CO2 to CH4 with an Organic Sensitizer and an Iron Porphyrin Catalyst. *J. Am. Chem. Soc.* **2018**, *140*, 17830−17834.
(30) Luo, S.-P.; Mejía, E.; Friedrich, A.; Pazidis, A.; Junge, H.; Surkus, A.-E.; Jackstell, R.; Denurra, S.; Gladiali, S.; Lochbrunner, S.; Beller, M. Photocatalytic Water Reduction with Copper-Based Photosensitizers: A Noble-Metal-Free System. *Angew. Chem., Int. Ed.* **2013**, *52*, 419−423.
(31) Rosas-Hernández, A.; Steinlechner, C.; Junge, H.; Beller, M. Earth-abundant photocatalytic systems for the visible-light-driven reduction of CO_2 to CO. *Green Chem.* **2017**, *19*, 2356−2360.
(32) Takeda, H.; Ohashi, K.; Sekine, A.; Ishitani, O. Photocatalytic CO_2 Reduction Using Cu(I) Photosensitizers with a Fe(II) Catalyst. *J. Am. Chem. Soc.* **2016**, *138*, 4354−4357.
(33) Takeda, H.; Monma, Y.; Sugiyama, H.; Uekusa, H.; Ishitani, O. Development of Visible-Light Driven Cu(I) Complex Photosensitizers for Photocatalytic CO_2 Reduction. *Front. Chem.* **2019**, *7*, 418.
(34) Zhang, X.; Cibian, M.; Call, A.; Yamauchi, K.; Sakai, K. Photochemical CO_2 Reduction Driven by Water-Soluble Copper(I) Photosensitizer with the Catalysis Accelerated by Multi-Electron Chargeable Cobalt Porphyrin. *ACS Catal.* **2019**, *9*, 11263−11273.
(35) Kiyosawa, K.; Shiraishi, N.; Shimada, T.; Masui, D.; Tachibana, H.; Takagi, S.; Ishitani, O.; Tryk, D. A.; Inoue, H. Electron Transfer from the Porphyrin S2 State in a Zinc Porphyrin-Rhenium Bipyridyl Dyad having Carbon Dioxide Reduction Activity. *J. Phys. Chem. C* **2009**, *113*, 11667−11673.
(36) Zhang, J.-X.; Hu, C.-Y.; Wang, W.; Wang, H.; Bian, Z.-Y. Visible light driven reduction of CO_2 catalyzed by an abundant manganese catalyst with zinc porphyrin photosensitizer. *Appl. Catal., A* **2016**, *522*, 145−151.
(37) Windle, C. D.; George, M. W.; Perutz, R. N.; Summers, P. A.; Sun, X. Z.; Whitwood, A. C. Comparison of rhenium-porphyrin dyads for CO_2 photoreduction: photocatalytic studies and charge separation dynamics studied by time-resolved IR spectroscopy. *Chem. Sci.* **2015**, *6*, 6847−6864.
(38) Kuramochi, Y.; Fujisawa, Y.; Satake, A. Photocatalytic CO_2 Reduction Mediated by Electron Transfer via the Excited Triplet State of Zn(II) Porphyrin. *J. Am. Chem. Soc.* **2020**, *142*, 705−709.
(39) Kuramochi, Y.; Satake, A. Photocatalytic CO_2 Reductions Catalyzed by meso-(1,10-Phenanthrolin-2-yl)-Porphyrins Having a Rhenium(I) Tricarbonyl Complex. *Chem. —Eur. J.* **2020**, *26*, 16365−16373.
(40) Ozawa, K.; Tamaki, Y.; Kamogawa, K.; Koike, K.; Ishitani, O. Factors determining formation efficiencies of one-electron-reduced species of redox photosensitizers. *J. Chem. Phys.* **2020**, *153*, 154302.
(41) Hosokawa, N.; Ozawa, K.; Koike, K.; Tamaki, Y.; Ishitani, O. The main factor that determines the formation-efficiencies of photochemically derived one-electron-reduced species. *Chem. Sci.* **2025**, *16*, 4279−4289.
(42) Uoyama, H.; Goushi, K.; Shizu, K.; Nomura, H.; Adachi, C. Highly efficient organic light-emitting diodes from delayed fluorescence. *Nature* **2012**, *492*, 234−238.
(43) Wong, M. Y.; Zysman-Colman, E. Purely Organic Thermally Activated Delayed Fluorescence Materials for Organic Light-Emitting Diodes. *Adv. Mater.* **2017**, *29*, 1605444.
(44) Nakanotani, H.; Tsuchiya, Y.; Adachi, C. Thermally-activated Delayed Fluorescence for Light-emitting Devices. *Chem. Lett.* **2021**, *50*, 938−948.
(45) Singh, V. K.; Yu, C.; Badgujar, S.; Kim, Y.; Kwon, Y.; Kim, D.; Lee, J.; Akhter, T.; Thangavel, G.; Park, L. S.; Lee, J.; Nandajan, P. C.; Wannemacher, R.; Milián-Medina, B.; Lüer, L.; Kim, K. S.; Gierschner, J.; Kwon, M. S. Highly efficient organic photocatalysts discovered via a computer-aided-design strategy for visible-light-driven atom transfer radical polymerization. *Nat. Catal.* **2018**, *1*, 794−804.
(46) Villa, M.; Fermi, A.; Calogero, F.; Wu, X.; Gualandi, A.; Cozzi, P. G.; Troisi, A.; Ventura, B.; Ceroni, P. Organic super-reducing photocatalysts generate solvated electrons via two consecutive photon induced processes. *Chem. Sci.* **2024**, *15*, 14739−14745.
(47) Wang, Y.; Gao, X.-W.; Li, J.; Chao, D. Merging an organic TADF photosensitizer and a simple terpyridine-Fe(iii) complex for photocatalytic CO_2 reduction. *Chem. Commun.* **2020**, *56*, 12170−12173.
(48) Wang, Y.; Liu, T.; Chen, L.; Chao, D. Water-Assisted Highly Efficient Photocatalytic Reduction of CO_2 to CO with Noble Metal-Free Bis(terpyridine)iron(II) Complexes and an Organic Photosensitizer. *Inorg. Chem.* **2021**, *60*, 5590−5597.
(49) Droghetti, F.; Mantovani, A.; Natali, M. Light-Driven CO_2 Reduction Catalysis with Organic Thermally Activated Delayed

https://doi.org/10.1021/jacs.5c10614
J. Am. Chem. Soc. XXXX, XXX, XXX−XXX

Fluorescence (TADF) Sensitizers. *ChemCatChem* **2025**, *17*, No. e202500247.
(50) Droghetti, F.; Villa, L.; Sartorel, A.; Dell'Amico, L.; Ruggi, A.; Natali, M. Boosting Light-Driven CO_2 Conversion Into CO by a Polypyridine Iron(II) Catalyst Using an Organic Sensitizer. *ChemSusChem* **2025**, *18*, No. e202402627.
(51) Ma, F.; Luo, Z.-M.; Wang, J.-W.; Ouyang, G. Highly Efficient, Noble-Metal-Free, Fully Aqueous CO_2 Photoreduction Sensitized by a Robust Organic Dye. *J. Am. Chem. Soc.* **2024**, *146*, 17773−17783.
(52) Yang, Z.; Mao, Z.; Xie, Z.; Zhang, Y.; Liu, S.; Zhao, J.; Xu, J.; Chi, Z.; Aldred, M. P. Recent advances in organic thermally activated delayed fluorescence materials. *Chem. Soc. Rev.* **2017**, *46*, 915−1016.
(53) Bassan, E.; Inoue, R.; Fabry, D.; Calogero, F.; Potenti, S.; Gualandi, A.; Cozzi, P. G.; Kamogawa, K.; Ceroni, P.; Tamaki, Y.; Ishitani, O. Visible-light driven photocatalytic CO_2 reduction promoted by organic photosensitizers and a Mn(i) catalyst. *Sustainable Energy Fuels* **2023**, *7*, 3454−3463.
(54) Hore, J.; Broadhurst, R. W. Photo-CIDNP of biopolymers. *Prog. Nucl. Magn. Reson. Spectrosc.* **1993**, *25*, 345−402.
(55) Verhoeven, J. W. On the role of spin correlation in the formation, decay, and detection of long-lived, intramolecular charge-transfer states. *J. Photochem. Photobiol. C* **2006**, *7*, 40−60.
(56) Wang, C.; Li, H.; Bürgin, T. H.; Wenger, O. S. Cage escape governs photoredox reaction rates and quantum yields. *Nat. Chem.* **2024**, *16*, 1151−1159.
(57) Goodwin, M. J.; Dickenson, J. C.; Ripak, A.; Deetz, A. M.; McCarthy, J. S.; Meyer, G. J.; Troian-Gautier, L. Factors that Impact Photochemical Cage Escape Yields. *Chem. Rev.* **2024**, *124*, 7379−7464.
(58) Pellegrin, Y.; Odobel, F. Sacrificial electron donor reagents for solar fuel production. *C. R. Chim.* **2017**, *20*, 283−295.
(59) Song, Y.; Kim, Y.; Noh, Y.; Singh, V. K.; Behera, S. K.; Abudulimu, A.; Chung, K.; Wannemacher, R.; Gierschner, J.; Lüer, L.; Kwon, M. S. Organic Photocatalyst for ppm-Level Visible-Light-Driven Reversible Addition-Fragmentation Chain-Transfer (RAFT) Polymerization with Excellent Oxygen Tolerance. *Macromolecules* **2019**, *52*, 5538−5545.
(60) Zhu, X.-Q.; Zhang, M.-T.; Yu, A.; Wang, C.-H.; Cheng, J.-P. Hydride, Hydrogen Atom, Proton, and Electron Transfer Driving Forces of Various Five-Membered Heterocyclic Organic Hydrides and Their Reaction Intermediates in Acetonitrile. *J. Am. Chem. Soc.* **2008**, *130*, 2501−2516.
(61) Tamaki, Y.; Koike, K.; Morimoto, T.; Ishitani, O. Substantial improvement in the efficiency and durability of a photocatalyst for carbon dioxide reduction using a benzoimidazole derivative as an electron donor. *J. Catal.* **2013**, *304*, 22−28.
(62) Koizumi, H.; Chiba, H.; Sugihara, A.; Iwamura, M.; Nozaki, K.; Ishitani, O. CO_2 capture by Mn(I) and Re(I) complexes with a deprotonated triethanolamine ligand. *Chem. Sci.* **2019**, *10*, 3080−3088.
(63) Takeda, H.; Kamiyama, H.; Okamoto, K.; Irimajiri, M.; Mizutani, T.; Koike, K.; Sekine, A.; Ishitani, O. Highly Efficient and Robust Photocatalytic Systems for CO_2 Reduction Consisting of a Cu(I) Photosensitizer and Mn(I) Catalysts. *J. Am. Chem. Soc.* **2018**, *140*, 17241−17254.
(64) Hasegawa, E.; Seida, T.; Chiba, N.; Takahashi, T.; Ikeda, H. Contrastive Photoreduction Pathways of Benzophenones Governed by Regiospecific Deprotonation of Imidazoline Radical Cations and Additive Effects. *J. Org. Chem.* **2005**, *70*, 9632−9635.

https://doi.org/10.1021/jacs.5c10614
J. Am. Chem. Soc. XXXX, XXX, XXX−XXX